# Piezoresistivity in pyrolyzed coconut fiber

Mohammed Mudassir [a], Bushair Ali K [b], Ali Ahmadian [c,d], C.N. Shyam Kumar [a,*]

[a] Department of Materials Science and Engineering, National Institute of Technology Calicut, 673601, Kerala, India
[b] Department of Physics, Sullamussalam Science College, Areekode, 673639, Kerala, India
[c] Helmholtz Institute Ulm for Electrochemical Energy Storage, 89081, Ulm, Germany
[d] Karlsruhe Nano Micro Facility (KNMF), Karlsruhe Institute of Technology (KIT), 76344, Eggenstein-Leopoldshafen, Germany

*Keywords:*
Pyrolyzed carbon
Coconut fiber
Electrical conductivity
Piezoresistive behavior

A B S T R A C T

Pyrolyzed carbon materials give fascinating solutions for many problems in the current research world. The locally available organic wastes can be pyrolyzed and tuned for their properties for various applications. Coconut-based materials such as shell and fiber have shown promising results in different technological applications. However, a detailed study of the structural and property evolution of these materials has not been carried out yet. In this work, the evolution of conductivity and piezoresistivity of coconut fiber-derived carbon is studied. Coconut fiber is pyrolyzed at different temperatures 600 °C, (CCP600) 800 °C (CCP800) and 1000 °C (CCP1000) to produce carbon fiber. Electrical conductivity experiments show differences between CCP600, CCP800 and CCP1000, with CCP600 displaying much lower conductivity at approximately (0.7 S/m) compared to CCP800 ($1 \times 10^3$ S/m) and CCP1000 ($1.4 \times 10^3$ S/m). Conversely, CCP600 demonstrates impressive piezoresistive characteristics, exhibiting significant resistance changes even under minimal strain. The gauge factor for the coconut fiber-derived carbon was found to be 4.1 for CCP600, 1.0 for CCP800, and 0.3 for CCP1000. Further, the powdered carbon samples show an increase in the gauge factor to a range of 36.8, which makes CCP600 well-suited for sensor applications requiring precise sensing capabilities. The present study suggests that CCP600, with its low cost and ease of fabrication, is a promising material for low-budget sensor applications.

## 1. Introduction

Pyrolyzed carbon materials have emerged as exciting candidates in various areas of research towards usability in micro and nano devices [1–3]. Researchers have carried out pyrolysis of organic materials to synthesize graphite/graphene-like materials with interesting mechanical, electrical, and thermal properties, to name a few [4–6]. The properties of these pyrolyzed materials can be tuned by varying the pyrolysis temperature making it suitable for various technological applications in battery electrodes [7], supercapacitors [8], dye-sensitized solar cell [9] water filtration or adsorbents [10], carbon fibres [11,12], etc. Notably, the structure and properties of these carbon materials are also affected by the source used, which can be diverse, ranging from cokes and pitches to polymers and organic matter.

Recently, studies have focused on the facile synthesis of carbon materials by the pyrolysis of organic wastes because of its abundance, low cost, and eco-friendly nature[9,13–16]. Out of these different organic wastes, coconut shells and coconut fibers are widely studied for different applications [17–20]. Due to its high surface area and porous nature, the coconut-based activated carbon fibers are used in applications such as efficient adsorption of organic dyes [21,22]. The carbon fibers were prepared via carbonization at 600 °C and KOH activation at 900 °C. It was found that the activation process increases the specific surface area of the carbon fibers. The maximum adsorption capacities were, 22.1, 20.7 and 21.3 mg $g^{-1}$, respectively for, Congo red, neutral red systems, and methylene blue [21,22]. The research carried out on transforming coconut fiber waste to graphitic carbon using nickel particles as a catalyst showed promising results as a gas diffusion layer [GDL] in proton exchange membrane fuel cell (PEMFC). The study used a Ni-based catalyst and the pyrolysis was carried out at 1300 °C for 3 h. The results show a transformation from amorphous to ordered graphitic nanostructure at 1200 °C. This structural change enhanced the electrical conductivity of carbon from 14.97 to 25.75 S/cm [23]. Researchers have also explored its applications in fields like wave absorption. The coconut fibers are extracted from the husk and activated using a KOH solution at 750 °C. The study attained an optimal reflection loss of 45.6 dB at 10.96 GHz with a corresponding effective bandwidth of 3.5 GHz at a thickness of 3.0 mm [24]. For Battery electrodes, the biomass-derived

* Corresponding author.
*E-mail address:* shyam@nitc.ac.in (C.N.S. Kumar).

carbon is used as high-performing nano-graphite at 850 °C. The samples show an electrochemical performance of ~200 mA h $g^{-1}$ at 5C for 1000 cycles (1C = 372 mA $g^{-1}$) as a fast-charging anode for lithium-ion batteries [25]. For supercapacitors, the activated carbon (AC) was mixed with KOH and activated at 400 °C for 1 h and 800 °C for 3 h. The capacitance increased significantly up to 46-fold, from 3.22 to 148.20 F/g [26]. Most of these studies use a two-step synthesis method in which after the first pyrolysis to intermediate temperatures, the fibers are powdered and pyrolyzed to higher temperatures and the initial aspect ratio is not maintained. By direct one-step synthesis, coconut fibers can be converted into carbon fibers with properties comparable to commercially available ones. Studies on the microstructural evolution during pyrolysis, reveal a similar graphitization pathway to polymer derived carbon fibers [27]. This similarity in graphitic content suggests a potential for piezoresistive behavior, as observed in unmodified PAN-based carbon fibers [28].

Piezoresistive behavior refers to the change in electrical resistance with mechanical strain. It enables resistance-based sensing of strain or stress and is quantified by the gauge factor (GF), defined as the fractional change in resistance per unit strain [29]. Conor and Owston were the first to study the inherent piezoresistive behavior of single carbon and reported a gauge factor between 0.7 and 1. The study found that the resistance increases with the tensile strain and related these changes with the degree of misorientation between crystallites [30]. Later, Berg et al. carried out experiments in carbon fibers and observed piezoresistive behavior during the stretching of carbon fibers with different modulus. The resistance increased when the mechanical tensile strain is applied for low-modulus material and the resistance of high-modulus fiber decreased with the tensile strain [31]. Endo et al. proposed that the resistivity changes may originate from the contact resistance of grain boundaries or the effect of stress on the electrical conduction in graphite planes [32]. Blazewicz et al. examined the piezoresistivity effect in different carbon fibers, they observed that the piezoresistivity effect is positive for carbon fibers with relatively small crystallite sizes and higher tensile strain [33]. Xi et al. observed the resistance-self-sensing ability of unmodified PAN-based carbon fibres with piezoresistive behavior. The gauge factor was found to be negative at two different strain ranges $406 \pm 20$ at strains ranging from 0 to 0.021 % and 1914 $\pm$ 140 at strains ranging from 0.021 % to 0.042 % [34]. These studies confirm the piezoresistive response in carbon fibers and gives a potential to explore piezoresistive behavior in materials with similar graphitic content.

There are also studies on the evolution of piezoresistive behavior in pyrolyzed carbon. The effect of tensile stress on the piezoresistive response of R10993-derived polymeric carbon was investigated by Hunt et al. [30]. The piezoresistance coefficient (resistance variation with the function of stress) for the pyrolyzed carbon at 600 °C was 5x$10^{-10}$ $m^2N^{-1}$ and became zero at 1200 °C. The study proposed that during heating, the piezoresistive behavior is obtained by the change in the band structure of the material [30]. But this consideration was based on a ribbon-like model of glassy carbons which is not energetically favorable at higher temperatures [35,36]. Stritt et al. investigated long-range conductivity mechanisms in SU-8 3005 photoresist-derived glassy carbon. They used the Van der Pauw technique, Broadband Coaxial Probe (BCP) and Microwave Cavity Perturbation (MCP)methods for measuring the DC conductivity. There was an exponential increase in conductivity in all methods that is expected for a disordered material above the percolation threshold [37]. Wang et al. made carbonized silk fabric strain sensor that shows a gauge factor (GF) of 5.8 even for very small strains in the range of 0–1% [38]. Jang et al. studied the SU-8-derived glassy carbon (GC) MEMS strain sensor pyrolyzed to 700 °C and 900 °C and reported a gauge factor of 2 for GC900 and 3.5 for GC700. The study correlates the increase in the in-plane size of the $sp^2$ cluster (La) and the alignment of fullerene-like layers at high temperatures to the intrinsic piezoresistivity of the glassy carbon [39]. The piezoresistive response was also observed in pyrolyzed thin films. Nano crystalline graphene prepared from microposit S1805 positive photoresist show promising piezoresistive response with a gauge factor of order 20 [40].

These studies show the possibility of piezoresistive response in pyrolyzed carbons. However, there are only limited investigations into the origin of piezoresistive behavior and its correlation with microstructural evolution in pyrolyzed carbon. Moreover, there are no reported studies on the piezoresistive behavior in coconut fiber pyrolyzed carbon (CCP). The present study aims to understand the evolution of inherent piezoresistive behavior in coconut fiber-derived pyrolyzed carbons. The study also explores the piezoresistive nature of pyrolyzed carbon powders from coconut fiber at different temperatures.

## 2. Materials and methods

### 2.1. Preparation of pyrolyzed carbon fibers

Coconut fibers were collected from the local manufacturing unit in Calicut, India. Initially washed using tap water, rinsed using DI water, and dried in the hot air oven at 150 °C for 1 h to remove any moisture present. The pyrolysis of coconut fiber was done at different temperatures under an Argon gas environment using a tubular furnace (Thermo Scientific, Thermolyne, USA). The pyrolysis was carried out at 600 °C, 800 °C and 1000 °C. The heating rate was 10 °C/min with a holding time of 5 h at the pyrolysis temperature.

### 2.2. Sample preparation for conductivity and piezoresistivity measurements of single-fiber

The CCP600, CCP800, and CCP1000 samples were pyrolyzed and separated as shown in Fig. 1. A 0.15 mm thickness polyvinyl chloride (PVC) sheet was used as a substrate. The thickness of the fiber was measured using an optical microscope. The CCP fibers were connected to a copper wire of 0.17 mm dia. using silver paste and cured using a hotplate at 50 °C for 30 min.

A commercially available adhesive (Fevicol from Pidilite Industries Ltd., India) was applied to the fiber to attach it firmly to the substrate. The microstructure of coating and bonding of single fiber on PVC and adhesive is studied (Given in Supplementary Information Fig. SI1). It was found there was no gap between the fiber and the substrate.

### 2.3. Sample preparation for piezoresistivity measurements of powdered samples

The pyrolyzed samples were powdered to fine size using mortar and pestle. The particle size of CCP powder ranges from 3 μm to 10 μm (Supplementary Information Fig.SI2). The 0.15 mm thick PVC sheet was sized into a square of 300 mm then a 250 × 200 mm shape was drawn on the substrate. To ensure the powder is added evenly, adhesive tape was fixed on four sides over the marked line leaving a space in the center. A commercially available adhesive (Fevicol from Pidilite Industries Ltd., India) was applied over the marked space, above which the powder was added and the remaining powder on the top was removed. The powder attached to the adhesive is cast tightly and allowed to settle. This process ensures a similar powder thickness to that of the adhesive tape for all samples. The cross-section images of sample CCP600, CCP800 and CCP1000 were analyzed to confirm the thickness of the powder and the bonding between the substrate, adhesive and powder. (Supplementary Information Fig.SI3). Then the copper wire was attached using silver paste and allowed to cure using a hotplate at 50 °C for 30 min.

### 2.4. Piezoresistivity measurements

The piezoresistivity measurements were carried out using a custom-made *in situ* micro tensile tester which is set up as shown in Fig. 2. The sample was loaded between the grips and a compressive force was applied to bend the substrate and the corresponding readings of

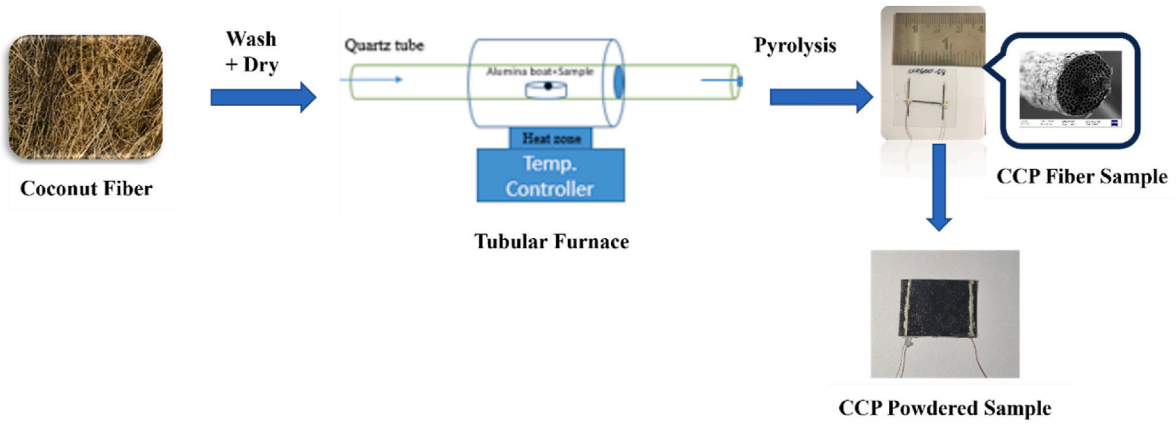


**Fig. 1.** Schematic representation of the synthesis of coconut fiber-derived carbon.

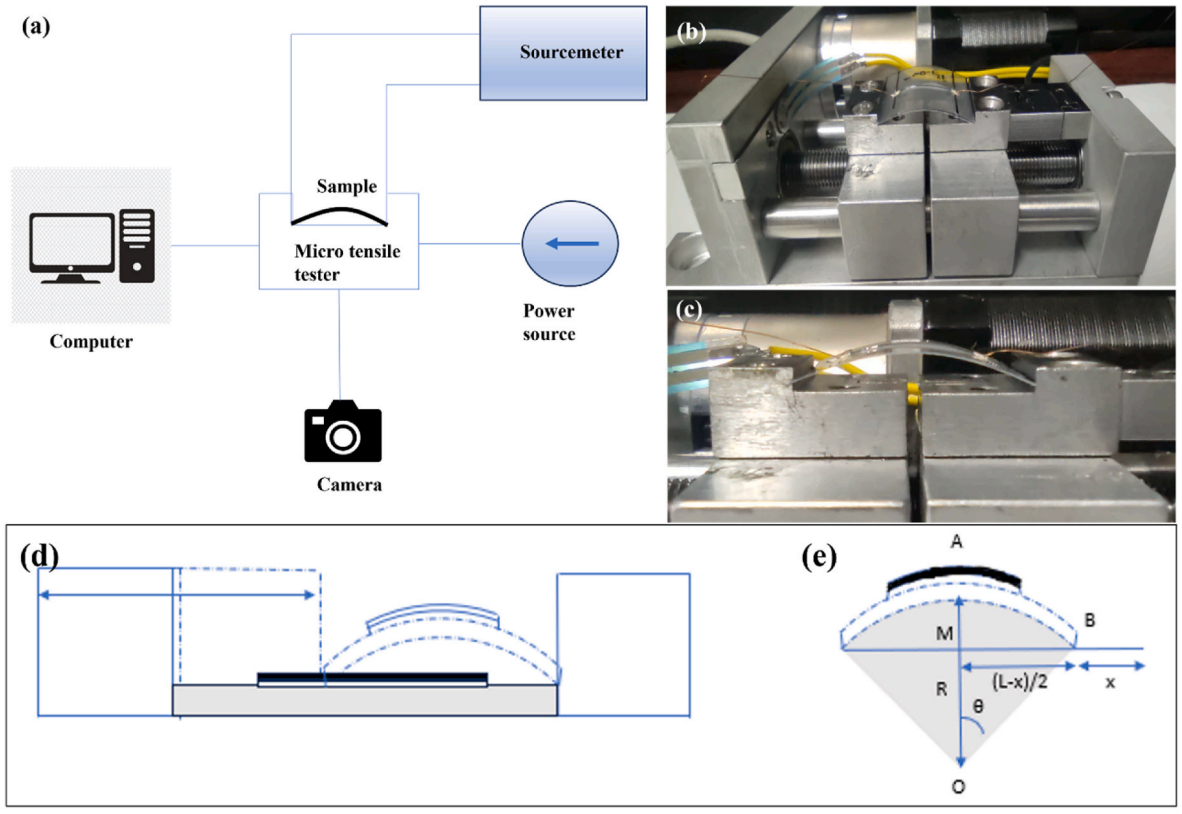


**Fig. 2.** (a) Schematic representation of setup used in testing piezoresistivity of the pyrolyzed carbon fiber. (b), (c) images of the bending experiment. (d) Schematic representation of the bending experiment. (e) initial (continuous) and final (dotted) curvature of the substrate during a lateral movement of x.

resistance were noted using a source meter [41]. Using resistance values and strain values, the gauge factor was calculated as described in Sandeep et al. [42]. The graph was plotted between change in resistance (ΔR/Ro) vs strain %. The gauge factor was calculated from the slope value using the linear fit method in the Origin software.

### 2.5. *Material characterization*

The morphological studies have been carried out in Secondary Electron (SE) mode using a Hitachi SU6600 Field Emission Scanning Electron Microscope (FE-SEM) with an acceleration voltage of 3 KV and 11 KV and using Carl Zeiss Gemini 1, Sigma 300, Germany (FE-SEM) with acceleration voltage 2 KV, equipped with an energy dispersive X-ray spectroscope (SMART EDX, Carl Zeiss). The degradation study was carried out using Thermogravimetric analysis TGA and Differential Thermogravimetry DTG analysis (Hitachi, STA 7200 Model). The surface area analysis was done using the BET setup (SmartSorb 93, Smart Instruments Company Private Limited, India). Raman studies were carried out using a confocal Raman Spectrometer (LABRam HR Evolution, HORIBA Scientific, Japan) with a laser excitation wavelength of 532 nm. XRD analysis of the pyrolyzed sample was conducted using an X-ray diffractometer (PANalytical Xpert3, Netherlands) with Cu Kα radiation (λ = 1.5406 Å). High-resolution transmission electron microscopy (TEM) and selected area electron diffraction (SAED) were carried out using a double aberration $C_s$-corrected TFS Themis Z (ThermoFisher Scientific) equipped with the Gatan OneView CMOS camera. The resistance of the pyrolyzed fiber was measured using a two-point probe system (Keithley Model 2450 Source Meter® SMU Instrument,

Tektronix, USA). The thickness of the fiber was measured using the optical microscope (RXLR-5, Radical, India).

## 3. Results and discussions

### 3.1. Raman spectra and TEM analysis

Fig. 3 a, shows the Raman spectra of the pyrolyzed coconut fiber. The G band, measured in the range of 1590–1595 cm $^{1}$ corresponds to the in-plane stretching mode of $sp^2$-bonded carbon. The D band is observed in the range of 1342-1337.7 cm $^{1}$ corresponds to the breathing mode of the $sp^2$ aromatic rings. The rise in the intensity of D peak is observed here from CCP600 to CCP1000 which leads to an increase in the $I_d/I_g$ ratio.

The $I_d/I_g$ ratio increased from 0.77 to 0.93, and 1.025 for CCP600, CCP800, and CCP1000 respectively. An increase in the $I_d/I_g$ ratio confirms the increasing graphitic domains in the material. The structure of the starting material plays a major role here. It consists of cellulose, hemicellulose and lignin. Lignin is an amorphous, highly branched and heterogeneous aromatic polymer [43]. During pyrolysis, after the initial carbonization, a carbonaceous structure is formed consisting of $sp^2$-bonded aromatic rings and the disorder carbon. This will be a starting skeleton for the graphitization process.

Further, with the temperature increase, the attachment of disordered carbon towards the edges of $sp^2$ carbon crystallites occurs. This $sp^3$ to $sp^2$ conversion increases the in-plane correlation length or crystallite size ($L_a$) increasing the ordered $sp^2$ graphitic domains. There will be a transformation from amorphous or disordered carbon to a less defective organized graphene-like structure with smaller $L_a$ [44]. This length $L_a$ is proportional to the number of aromatic rings present in the material. In the case of amorphous material, the D band strength is proportional to the probability of finding a six-fold aromatic ring in the material. With the increase in aromatic rings, the D band strength increases and the $I_d/I_g$ ratio increases [45].

Fig. 3b-d shows high-resolution TEM images of pyrolyzed coconut fiber. The microstructural evolutions of the graphitic domains are observed with an increase in temperature. This is consistent with the Raman characterization that the increase in the $I_d/I_g$ ratio represents the growth of in-plane correlation length $L_a$ of $sp^2$ graphitic domains. After the initial carbonization, further graphitization proceeds in two ways. This is by the attachment of the disordered carbon to the edges of the crystallites and by the ordering and merging of the crystallites, which leads to an increase in crystallite size [6]. The evolution of curved $sp^2$ graphitic domains with few graphene-like layers is visible in the TEM images. The Selected Area Electron Diffraction (SAED) patterns show two rings, (100) and (110) correspond to characteristics of

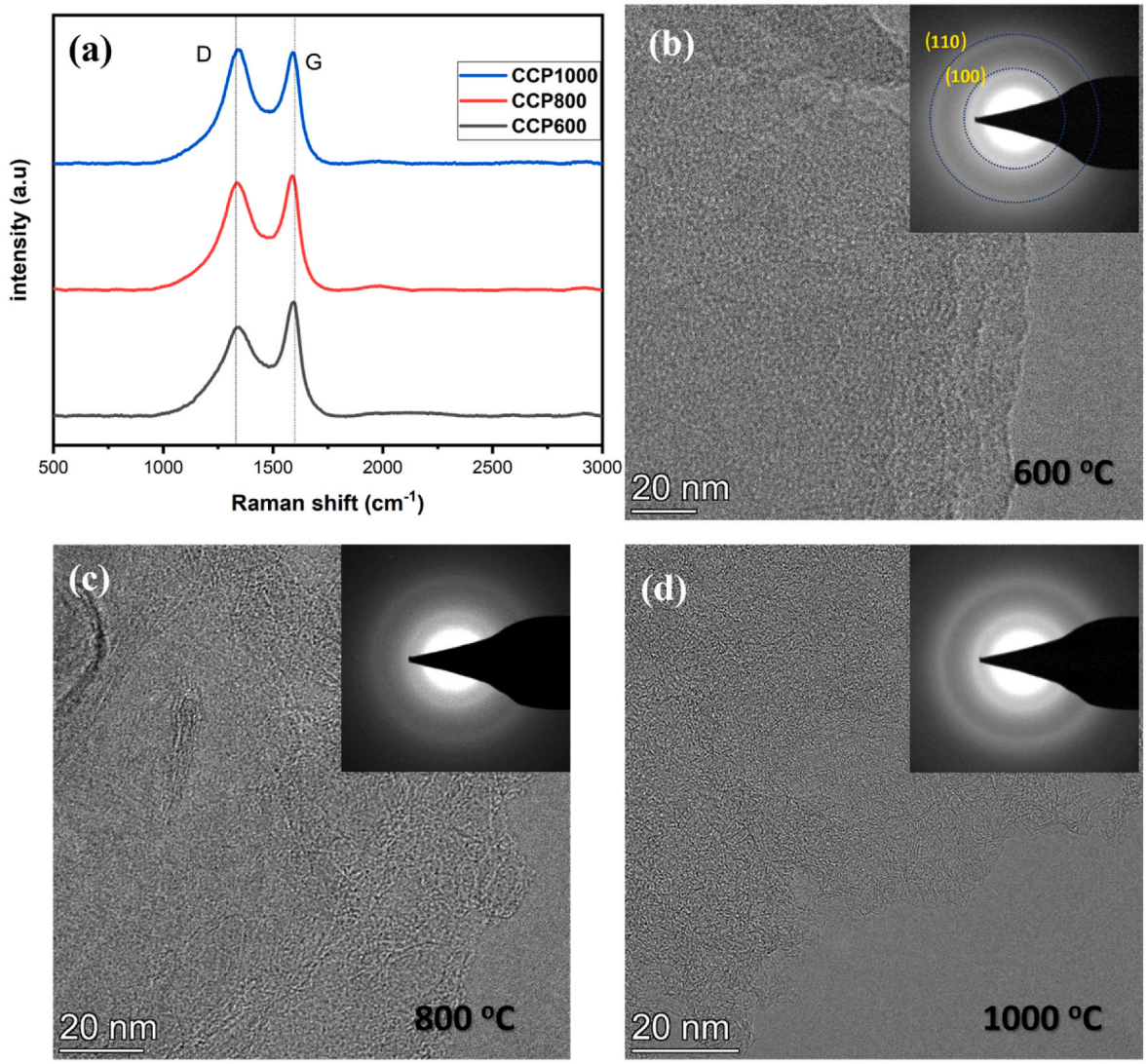


**Fig. 3.** (a) Raman spectrum of coconut fiber-derived carbon. (b), (c) &(d) High-resolution TEM images of pyrolyzed fiber-derived carbon at different temperatures. The insets show the corresponding SAED pattern, where the marked (100) and (110) rings become sharper with increasing temperature.

$sp^2$-hybridized carbon materials [46]. It can be also observed that the rings are becoming sharper with the increase in the pyrolysis temperature which shows the formation of a more ordered structure. The crystallite size was calculated from the intensity profiles of the SAED patterns using the Scherrer equation [47–49]. The crystallite size was found to be 2.8 nm for the CCP 1000 sample. The calculated crystallite size is comparable with previous studies on polymer-derived glassy carbon/nanocrystalline graphene [48,50]. From the XRD studies (Given in Supplementary Information Fig.SI4) a broad (002) peak and (100) peak is observed in the regions $26^o$ and $44^o$ which also shows the graphitic nature of pyrolyzed carbon.

### 3.2. SEM analysis

Fig. 4a-c shows the low magnification SEM images of the pyrolyzed coconut fibers at different temperatures. The SEM images indicate an influence of the temperature on the topography of the fiber surface. The evolution of pores can be observed at higher temperatures. From the cross-section images of these pyrolyzed fibers (Given in Supplementary Information Figure SI5), a narrow, hollow tube-like structure is visible. This structure depicts the pathway through which water molecules and minerals move. It is to be noted that the tubular structure is not altered after the pyrolysis to high temperatures.

Additionally, bright spherical particles identified as silica particles were seen fused over the surface. These silica particles are also observed at higher temperatures. In certain regions, these silica particles are completely absent leaving circular-shaped pits with pores on the fiber surface (Supplementary Information Figure SI6). The silica particles on the surface can be removed using an aqueous NaOH solution (Supplementary Information Figure SI7). In this study, silica etching was not carried out for piezoresistive measurements.

During pyrolysis, the main cell wall components such as cellulose, hemicellulose and lignin start decomposing. This is also confirmed using the TGA analysis (Given in the Supplementary Information Fig.SI8). Decomposition of abundant adjacent hydroxyls in both cellulose and hemicellulose produce micropores while aromatic p-hydroxy phenyl, guaicyl and syringyl units from lignin form non-microporous $sp^2$ structures [51]. Fig. 4 d-f shows higher magnification images of the increasing porosity at increasing temperatures. The extent of pore formation will depend on the heating temperature, heating duration and rate of heating.

The surface area analysis was done for pyrolyzed carbon at different temperatures. For CCP600 surface area was 341.6 $m^2/g$ which is raised to 814.3 $m^2/g$ for CCP800 and 1200 $m^2/g$ for CCP1000. The increase in the surface area confirms the increase in the porosity at elevated temperatures.

### 3.3. Electrical conductivity and piezoresistive study of single-fiber

The sample prepared for the electrical conductivity and piezoresistive measurements is shown in Fig. 5 a. Fig. 5 b shows the image of the in-house built micro tensile tester setup. Fig. 5. C shows the electrical conductivity of the samples at different temperature. In CCP600 the electrical conductivity is $0.7 \pm 0.5$ S/m which increased to $1069 \pm 19$ S/m in CCP800 and $1493 \pm 25$ S/m in CCP1000. Fig. 5d shows the maximum observed GF for the fiber samples which is 4.1 for CCP600, 1.0 for CCP800 and 0.3 for CCP1000. Fig. 5e gives the average value of the GF with a standard deviation of samples indicating a GF of $2.7 \pm 0.9$ for CCP600, $0.6 \pm 0.2$ for CCP800 and $0.3 \pm 0.1$ for CCP1000. The results demonstrate the inherent piezoresistive nature of coconut fiber-derived carbon. The piezoresistive response is higher for CCP600 and decreases with increasing pyrolysis temperature. The results agree with the previous studies which showed an increase in electrical conductivity and a decrease in piezoresistivity (GF) with increasing pyrolysis temperature.

The increase in conductivity can be attributed to the increase in the $sp^2$ content which increases the in-plane size of the $sp^2$ cluster (La). The increase La and the alignment of crystallites at high temperatures which affects the conductivity and intrinsic piezoresistivity of the glassy carbon [39]. The structure of pyrolyzed carbon at lower pyrolysis temperatures consists of conducting $sp^2$ graphitic domains dispersed in an insulating $sp^3$ matrix. As the temperature increases, the attachment of disordered carbon towards the edges of $sp^2$ carbon crystallites occurs [52]. This $sp^3$ to $sp^2$ conversion increases the in-plane correlation length or crystallite size ($L_a$) increasing the ordered $sp^2$ graphitic domains. There will be a transformation from amorphous carbon or disordered carbon to a less defective organized graphene-like structure with smaller $L_a$. The conductivity in the pyrolyzed carbon can be explained by the proposed tunneling model, which says that the tunneling of electrons between the conductive $sp^2$ clusters occurs when the distance between

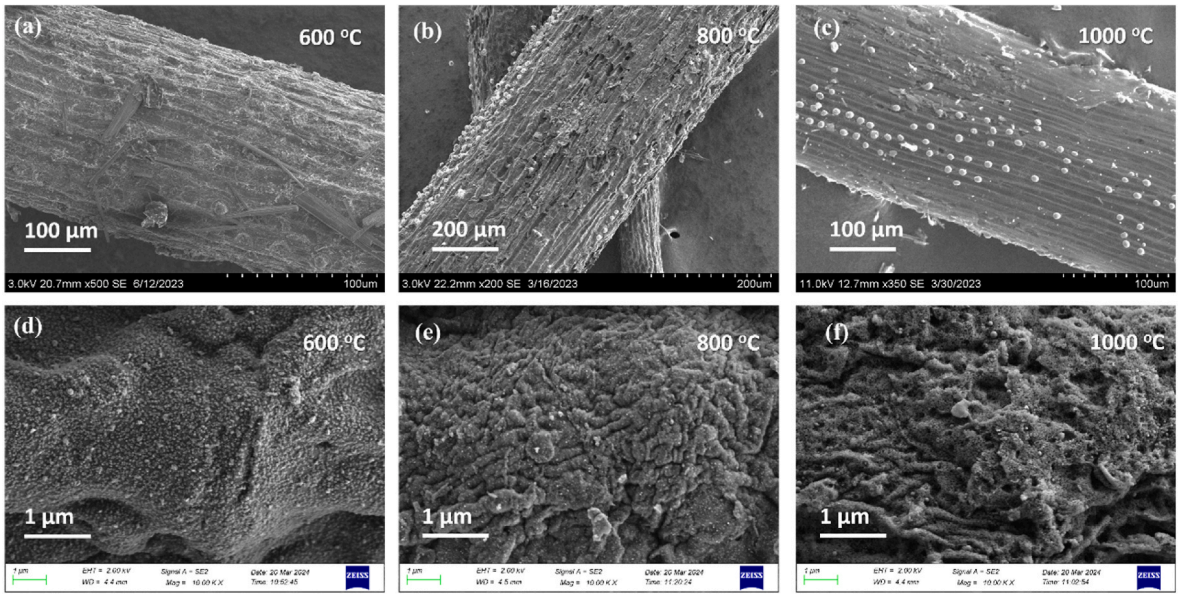


**Fig. 4.** (a–c): SEM images of pyrolyzed carbon fiber at different temperatures. The images show the morphological changes and evolution of silica particles at different temperatures. (d–f): High magnification surface image of CCP600, CCP800 and CCP1000 samples showing the evolution of porosity on the surface.

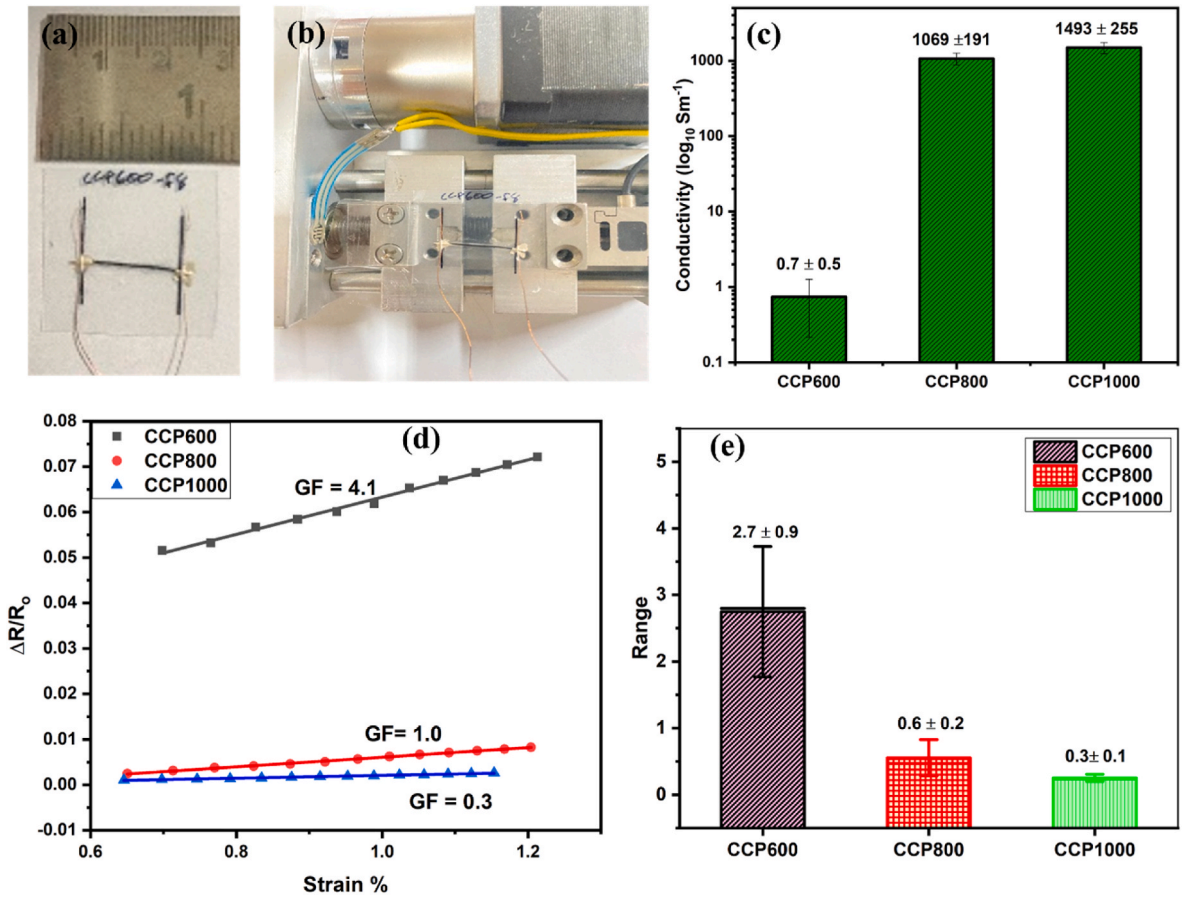


**Fig. 5.** (a) The prepared fiber sample (b) The sample loaded between the *in situ* micro tensile tester (c) The bar diagram showing the electrical conductivity of the fiber samples (d) Maximum observed GF of fiber samples (e) The Error bar graph for the GF of fiber samples.

the conductive particles is small and the electron wave functions from two conductors overlap inside the insulating material [53].

Here the electrons tunnel between two $sp^2$ graphitic domains in insulating $sp^3$ matrix as shown in Fig. 6. As the temperature increases in CCP800 and CCP1000, the growth of ordered $sp^2$ graphitic domains occur reducing the gap between these domains. This will reduce the tunneling distance of the electrons. This reduced barrier leads to lower electrical resistance and consequently, improved conductivity.

As explained above, the piezoresistive behavior is also linked to the change in the tunneling distance between the conducting $sp^2$ graphitic domains in the insulating $sp^3$ matrix [54,55]. During bending, the induced strain increases the gap between $sp^2$ graphitic domains, hindering electron movement and increasing resistance. This change in resistance results in the inherent piezoresistive nature of the pyrolyzed coconut fiber.

At higher temperatures, as explained above the tunneling distance is reduced due to the growth of $sp^2$ graphitic domains. The variation in the tunneling distance is also reduced during the bending. The resistance

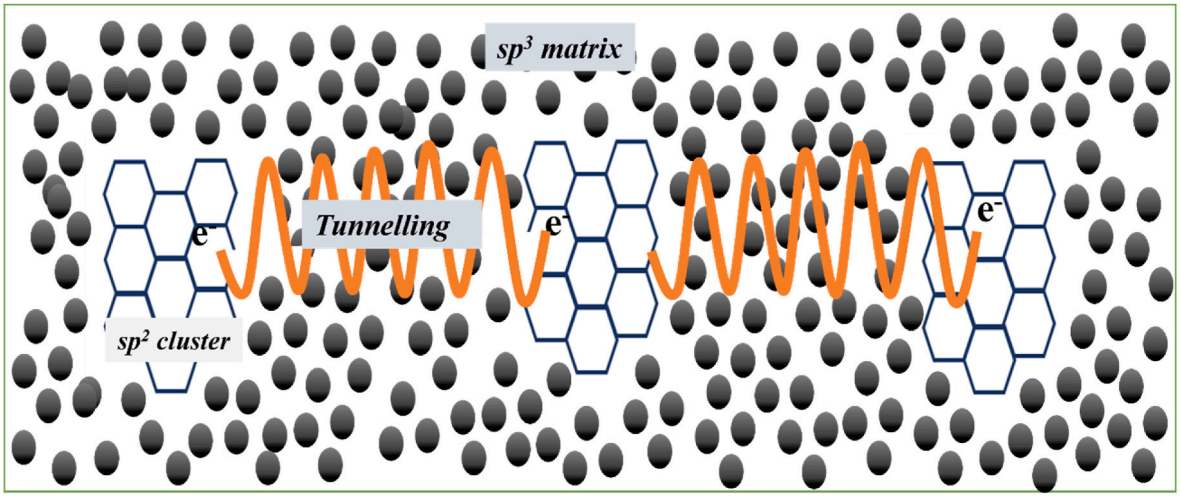


**Fig. 6.** Electron transfer in pyrolyzed single carbon fiber sample.

change is lesser compared to in the lower temperature. This results in lesser piezoresistivity and corresponding lower gauge factors at higher temperatures.

### 3.4. *Piezoresistive behavior of CCP powder*

The schematic and the sample prepared using coconut-derived pyrolyzed carbon powder can be observed in Fig. 7 a and 7. b respectively. Fig. 7 c. shows the piezoresistive response of the powdered samples. The GF was increased in all the powdered samples compared to single fiber. CCP600 has the highest GF of 36.8, which decreases to 21 for CCP800 and 8.4 for CCP1000. Fig. 7d gives the average with a standard deviation of samples indicating a GF for 29.8 ± 5.6 for CCP600, 17.5 ± 3.2 for CCP800 and 5.2 ± 2.4 for CCP1000.

In powder samples, the GF value observed is high compared to the single fiber samples. This can be due to the presence of the contact resistance between the particles in addition to the tunneling resistance (Given in Supplementary Information Figure SI 9). The contact between two fiber particles causes an increase in resistance. During normal conditions, the conducting pathway is more with a greater number of contacts between the fiber. While bending, some of the contact breaks and the resistance increases. This causes a total increase in the resistance change of the sample further to a higher level.

The present study confirms the inherent piezoresistive property in coconut fiber-derived carbon. Temperature-dependent piezoresistivity makes it easier to adjust the piezoresistive response for various uses. The inherent piezoresistivity in coconut fiber derived carbon will open new possibility where the locally available coconut wastes can be utilized as the sensing devices. This may include the fabrication of touch sensors, pressure sensors etc. which can be tuned according for various applications in automobile, aerospace and medical fields.

## 4. Conclusion

The study focuses on the correlation of microstructure, morphology and piezoresistivity of pyrolyzed coconut fiber. Coconut fiber is pyrolyzed at different temperatures 600 °C, (CCP600) 800 °C (CCP800) and 1000 °C (CCP1000) to produce carbon fiber. The microstructural evolution of the pyrolysis was studied in detail. The formation of $sp^2$ graphitic regions in the $sp^3$ matrix was confirmed by Raman Spectroscopy. The surface morphology of the fiber also changed with higher temperatures and showed the evolution of porosity. Conductivity experiments show that the electrical conductivity increases with increasing pyrolysis temperature. The sample pyrolyzed to 600° (CCP 600) displaying lower conductivity at approximately 0.745 S/m. The conductivity increased to $1.06 \times 10^3$ S/m for CCP800 and $1.4 \times 10^3$ S/m for CCP1000.

Piezoresistive studies on single carbon fiber derived from coconut fiber show that CCP600 have inherent piezoresistive characteristics, exhibiting significant resistance changes even under minimal strain. The maximum GF was found to be 4.1 for CCP600, 1.0 for CCP800 and 0.3 for CCP1000 single fiber. Further, an increase in the gauge factor in CCP powdered samples to a range of 36 for CCP600, 21 for CCP800 and 8 for CCP1000 was observed.

The study suggests that CCP600, with its low cost and ease of fabrication, is a promising material for low-budget sensor applications. Understanding these material-specific properties facilitates informed material selection for optimal functionality in diverse applications.

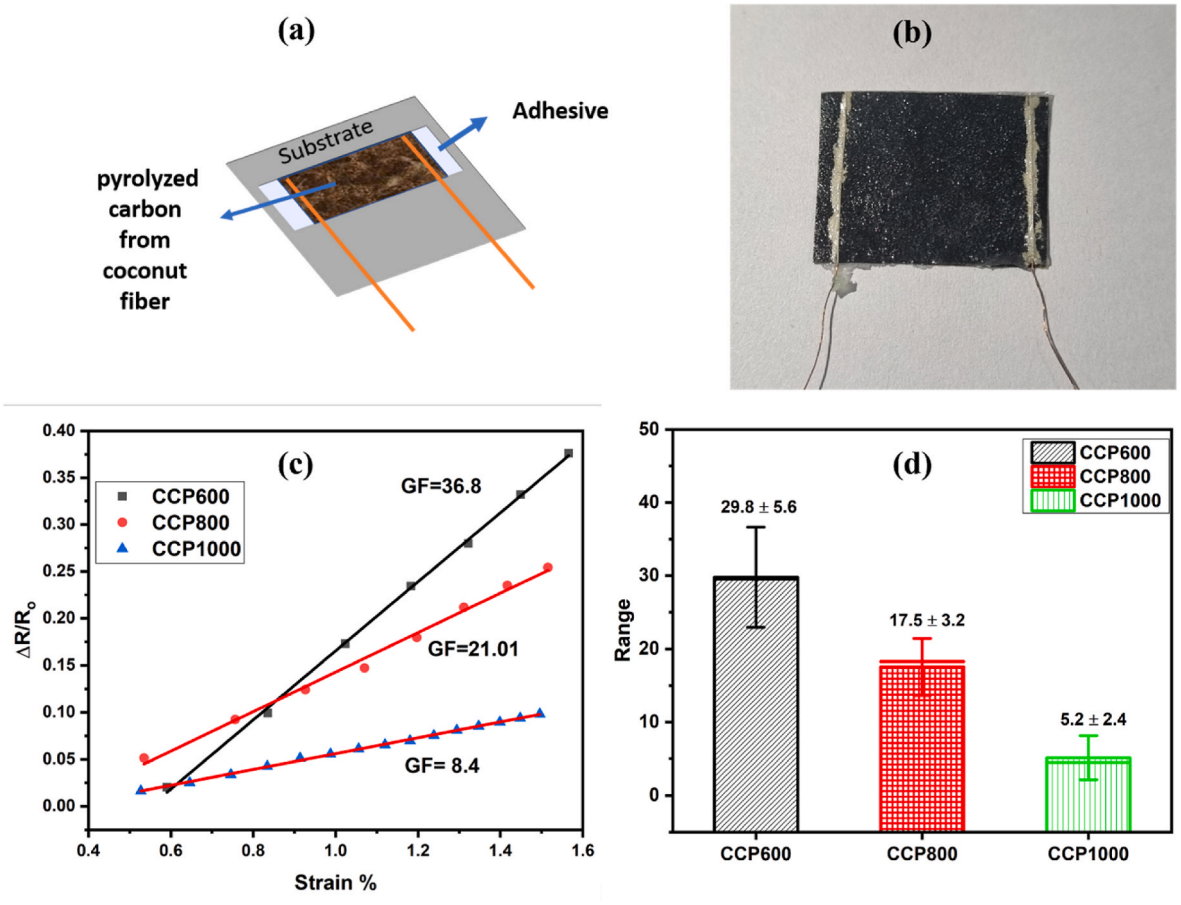


**Fig. 7.** (a) Schematic of the powdered carbon sample. (b) The sample prepared for testing (c). Maximum observed GF of powdered samples. (d) The average value with standard deviation.

.

Further research into CCP600's piezoresistive behavior could unlock additional insights, enhancing its sensor capabilities and expanding its potential applications.

## CRediT authorship contribution statement

**Mohammed Mudassir:** Writing – review & editing, Writing – original draft, Visualization, Methodology, Investigation. **Bushair Ali K:** Methodology, Investigation. **Ali Ahmadian:** Methodology, Investigation. **C.N. Shyam Kumar:** Writing – review & editing, Supervision, Methodology, Conceptualization.

## Acknowledgement

The authors acknowledge the TEM measurements at the Karlsruhe Nano Micro Facility (KNMFi), a Helmholtz research infrastructure operated at Karlsruhe Institute of Technology (KIT), Karlsruhe, Germany. The authors would also like to acknowledge the FIST-funded (FIST - No. SR/FST/ET-I/2021/840) SEM Centre at the Department of Materials Science and Engineering at NITC for the SEM characterization, Central Raman Facility and Central XRD facility at NITC for carrying out Raman and XRD measurements. C.N. Shyam Kumar acknowledge the SING research grant from Indo German Science and Technology Center (IGSTC) for the design and fabrication of micro-tensile tester used for piezoresistive studies.

## Data availability

Data will be made available on request.

## References

[1] S. Sharma, S. Basu, N.P. Shetti, K. Mondal, A. Sharma, T.M. Aminabhavi, Versatile graphitized carbon nanofibers in energy applications, ACS Sustain Chem Eng 10 (2022) 1334–1360, https://doi.org/10.1021/acssuschemeng.1c06762.
[2] V. Uskoković, A historical review of glassy carbon: synthesis, structure, properties and applications, Carbon Trends 5 (2021) 100116, https://doi.org/10.1016/j.cartre.2021.100116.
[3] P.J.F. Harris, Fullerene-related structure of commercial glassy carbons, Phil. Mag. 84 (2004) 3159–3167, https://doi.org/10.1080/14786430410001720363.
[4] 95/04670 Carbon black science and technology. https://doi.org/10.1016/0140-6701(95)96467-q, 1995.
[5] S. Sharma, Glassy Carbon: a promising material for microand nanomanufacturing, Materials 11 (2018), https://doi.org/10.3390/ma11101857.
[6] S. Sharma, C.N. Shyam Kumar, J.G. Korvink, C. Kübel, Evolution of glassy carbon microstructure: in situ transmission electron microscopy of the pyrolysis process, Sci. Rep. 8 (2018) 1–12, https://doi.org/10.1038/s41598-018-34644-9.
[7] K. Yu, J. Li, H. Qi, C. Liang, High-capacity activated carbon anode material for lithium-ion batteries prepared from rice husk by a facile method, Diam. Relat. Mater. 86 (2018) 139–145, https://doi.org/10.1016/j.diamond.2018.04.019.
[8] E.Y.L. Teo, L. Muniandy, E.-P. Ng, F. Adam, A.R. Mohamed, R. Jose, K.F. Chong, High surface area activated carbon from rice husk as a high performance supercapacitor electrode, Electrochim. Acta 192 (2016) 110–119, https://doi.org/10.1016/j.electacta.2016.01.140.
[9] S. Xu, One-step fabrication of carbon fiber derived from waste paper and its application for catalyzing tri-iodide reduction, IOP Conf. Ser. Earth Environ. Sci. 52 (2017) 12014, https://doi.org/10.1088/1742-6596/52/1/012014.
[10] M. Ahmedna, W.E. Marshall, A.A. Husseiny, R.M. Rao, I. Goktepe, The use of nutshell carbons in drinking water filters for removal of trace metals, Water Res. 38 (2004) 1062–1068, https://doi.org/10.1016/j.watres.2003.10.047.
[11] P. Jagdale, E.P. Koumoulos, I. Cannavaro, A. Khan, M. Castellino, D. A. Dragatogiannis, A. Tagliaferro, C.A. Charitidis, Towards green carbon fibre manufacturing from waste cotton: a microstructural and physical property investigation, Manufacturing Rev 4 (2017), https://doi.org/10.1051/mfreview/2017008.
[12] L. de S. Vieira, A review on the use of glassy carbon in advanced technological applications, Carbon N Y 186 (2022) 282–302, https://doi.org/10.1016/j.carbon.2021.10.022.
[13] B.P. Thapaliya, H. Luo, P. Halstenberg, H.M. Meyer, J.R. Dunlap, S. Dai, Low-cost transformation of biomass-derived carbon to high-performing nano-graphite via low-temperature electrochemical graphitization, ACS Appl. Mater. Interfaces 13 (2021) 4393–4401, https://doi.org/10.1021/acsami.0c19395.
[14] N.M. Zúñiga-Muro, A. Bonilla-Petriciolet, D.I. Mendoza-Castillo, C.J. Duran-Valle, J. Silvestre-Albero, H.E. Reynel-Ávila, J.C. Tapia-Picazo, Recycling of Tetra pak wastes via pyrolysis: characterization of solid products and application of the resulting char in the adsorption of mercury from water, J. Clean. Prod. 291 (2021) 125219, https://doi.org/10.1016/j.jclepro.2020.125219.
[15] M.H. Al-Malack, A.A. Basaleh, Adsorption of heavy metals using activated carbon produced from municipal organic solid waste, Desalination Water Treat. 57 (2016) 24519–24531, https://doi.org/10.1080/19443994.2016.1144536.
[16] S. Yousef, R. Kalpokaitė-Dičkuvienė, A. Baltušnikas, I. Pitak, S.I. Lukošiūtė, A new strategy for functionalization of char derived from pyrolysis of textile waste and its application as hybrid fillers (CNTs/char and graphene/char) in cement industry, J. Clean. Prod. 314 (2021) 128058, https://doi.org/10.1016/j.jclepro.2021.128058.
[17] D. A, S.A.B.A. Manaf, Y. S, C. K, K. N, G. Hegde, Low cost, high performance supercapacitor electrode using coconut wastes: eco-friendly approach, J. Energy Chem. 25 (2016) 880–887, https://doi.org/10.1016/j.jechem.2016.08.002.
[18] J.Y. Yusuf, H. Soleimani, N. Yahya, Y.K. Sanusi, G. Kozlowski, A. Öchsner, L. L. Adebayo, F.A. Wahaab, S. Sikiru, B.B. Balogun, Electromagnetic wave absorption of coconut fiber-derived porous activated carbon, Bol. Soc. Espanola Ceram. Vidr. 61 (2022) 417–427, https://doi.org/10.1016/j.bsecv.2021.02.003.
[19] F. Fahmi, N.A.A. Dewayanti, W. Widiyastuti, H. Setyawan, Preparation of porous graphene-like material from coconut shell charcoals for supercapacitors, Cogent Eng 7 (2020), https://doi.org/10.1080/23311916.2020.1748962.
[20] S.S. Sekhon, P. Kaur, J.S. Park, From coconut shell biomass to oxygen reduction reaction catalyst: tuning porosity and nitrogen doping, Renew. Sustain. Energy Rev. 147 (2021) 111173, https://doi.org/10.1016/j.rser.2021.111173.
[21] L. Zhang, L.Y. Tu, Y. Liang, Q. Chen, Z.S. Li, C.H. Li, Z.H. Wang, W. Li, Coconut-based activated carbon fibers for efficient adsorption of various organic dyes, RSC Adv. 8 (2018) 42280–42291, https://doi.org/10.1039/c8ra08990f.
[22] H.A. AL-Aoh, R. Yahya, M. Jamil Maah, M. Radzi Bin Abas, Adsorption of methylene blue on activated carbon fiber prepared from coconut husk: isotherm, kinetics and thermodynamics studies, Desalination Water Treat. 52 (2014) 6720–6732, https://doi.org/10.1080/19443994.2013.831794.
[23] F. Destyorini, R. Yudianti, Y. Irmawati, A. Hardiansyah, Y.I. Hsu, H. Uyama, Temperature driven structural transition in the nickel-based catalytic graphitization of coconut coir, Diam. Relat. Mater. 117 (2021) 108443, https://doi.org/10.1016/j.diamond.2021.108443.
[24] J.Y. Yusuf, H. Soleimani, N. Yahya, Y.K. Sanusi, G. Kozlowski, A. Öchsner, L. L. Adebayo, F.A. Wahaab, S. Sikiru, B.B. Balogun, Electromagnetic wave absorption of coconut fiber-derived porous activated carbon, Bol. Soc. Espanola Ceram. Vidr. 61 (2022) 417–427, https://doi.org/10.1016/j.bsecv.2021.02.003.
[25] B.P. Thapaliya, H. Luo, P. Halstenberg, H.M. Meyer, J.R. Dunlap, S. Dai, Low-cost transformation of biomass-derived carbon to high-performing nano-graphite via low-temperature electrochemical graphitization, ACS Appl. Mater. Interfaces 13 (2021) 4393–4401, https://doi.org/10.1021/acsami.0c19395.
[26] F. Fahmi, N.A.A. Dewayanti, W. Widiyastuti, H. Setyawan, Preparation of porous graphene-like material from coconut shell charcoals for supercapacitors, Cogent Eng 7 (2020), https://doi.org/10.1080/23311916.2020.1748962.
[27] B.A. Newcomb, Processing, structure, and properties of carbon fibers, Compos Part A Appl Sci Manuf 91 (2016) 262–282, https://doi.org/10.1016/j.compositesa.2016.10.018.
[28] X. Xi, D.D.L. Chung, Piezoelectric and piezoresistive behavior of unmodified carbon fiber, Carbon N Y 145 (2019) 452–461, https://doi.org/10.1016/j.carbon.2019.01.044.
[29] A.S. Fiorillo, C.D. Critello, A.S. Pullano, Theory, technology and applications of piezoresistive sensors: a review, Sens Actuators A Phys 281 (2018) 156–175, https://doi.org/10.1016/j.sna.2018.07.006.
[30] D.R. Hunt, G.M. Jenkins, T. Takezawa, The effect of tensile stress upon the resistivity of a polymeric carbon, Carbon N Y 14 (1976) 105–109, https://doi.org/10.1016/0008-6223(76)90118-4.
[31] A. Rinsky, Piezoresistance Fibers, (n.d.) 486–489.
[32] T. Koyama, M. Endo, Electrical resistivity of carbon fiber prepared from benzene, Jpn. J. Appl. Phys., Part 1: Regular Papers and Short Notes and Review Papers 13 (1974) 1175–1176, https://doi.org/10.1143/JJAP.13.1175.
[33] S. Błazewicz, B. Patalita, P. Touzain, Study of piezoresistance effect in carbon fibers, Carbon N Y 35 (1997) 1613–1618, https://doi.org/10.1016/S0008-6223(97)00120-6.
[34] X. Xi, D.D.L. Chung, Piezoelectric and piezoresistive behavior of unmodified carbon fiber, Carbon N Y 145 (2019) 452–461, https://doi.org/10.1016/j.carbon.2019.01.044.
[35] V. Uskoković, A historical review of glassy carbon: synthesis, structure, properties and applications, Carbon Trends 5 (2021), https://doi.org/10.1016/j.cartre.2021.100116.
[36] S. Sharma, C.N. Shyam Kumar, J.G. Korvink, C. Kübel, Evolution of glassy carbon microstructure: in situ transmission electron microscopy of the pyrolysis process, Sci. Rep. 8 (2018) 1–12, https://doi.org/10.1038/s41598-018-34644-9.
[37] J. Stritt, J.A. Cuenca, E.L.H. Thomas, O.A. Williams, Development of long-range conductivity mechanisms in glass-like carbon, Carbon N Y 223 (2024) 119027, https://doi.org/10.1016/j.carbon.2024.119027.
[38] C. Wang, X. Li, E.L. Gao, M.Q. Jian, K.L. Xia, Q. Wang, Z.P. Xu, T.L. Ren, Y. Y. Zhang, Carbonized silk fabric for ultrastretchable, highly sensitive, and wearable strain sensors, Adv. Mater. 28 (2016) 6640–6648, https://doi.org/10.1002/adma.201601572.

[39] J. Jang, G. Panusa, G. Boero, J. Brugger, A GLASS-LIKE CARBON MEMS STRAIN SENSOR Microsystems Laboratory , École Polytechnique Fédérale de Lausanne (EPFL), Lausanne , Department of Functional Ceramics, vol. 1, Korea Institute of Materials Science (KIMS), Changwon , Optics Laboratory (LO), École Po, 2021, pp. 871–874.
[40] A. Riaz, F. Pyatkov, A. Alam, S. Dehm, A. Felten, V.S.K. Chakravadhanula, B. S. Flavel, C. Kübel, U. Lemmer, R. Krupke, Light emission, light detection and strain sensing with nanocrystalline graphene, Nanotechnology 26 (2015), https://doi.org/10.1088/0957-4484/26/32/325202.
[41] M.V. Swain, Plastic deformation of brittle materials, Key Eng. Mater. 166 (1999) 41–46.
[42] S. Kumar, Nanocarbon devices and sensors, PhD Thesis (2021). TUprints.
[43] K.C. Khaire, V.S. Moholkar, A. Goyal, Bioconversion of sugarcane tops to bioethanol and other value added products: an overview, Mater Sci Energy Technol 4 (2021) 54–68, https://doi.org/10.1016/j.mset.2020.12.004.
[44] C.N. Shyam Kumar, V.S.K. Chakravadhanula, A. Riaz, S. Dehm, D. Wang, X. Mu, B. Flavel, R. Krupke, C. Kübel, Understanding the graphitization and growth of free-standing nanocrystalline graphene using in situ transmission electron microscopy, Nanoscale 9 (2017) 12835–12842, https://doi.org/10.1039/C7NR03276E.
[45] A.C. Ferrari, J. Robertson, Raman spectroscopy of amorphous, nanostructured, diamond-like carbon, and nanodiamond, Phil. Trans. Math. Phys. Eng. Sci. 362 (2004) 2477–2512, https://doi.org/10.1098/rsta.2004.1452.
[46] H.D. Asfaw, C.-W. Tai, M. Valvo, R. Younesi, Facile synthesis of hard carbon microspheres from polyphenols for sodium-ion batteries: insight into local structure and interfacial kinetics, Mater. Today Energy 18 (2020) 100505, https://doi.org/10.1016/j.mtener.2020.100505.
[47] C. Oprea, V. Ciupina, G. Prodan, Investigation of nanocrystals using TEM micrographs and electron diffraction technique, Rom. Rep. Phys. 53 (2008) 223–230.
[48] C.N. Shyam Kumar, V.S.K. Chakravadhanula, A. Riaz, S. Dehm, D. Wang, X. Mu, B. Flavel, R. Krupke, C. Kübel, Understanding the graphitization and growth of free-standing nanocrystalline graphene using in situ transmission electron microscopy, Nanoscale 9 (2017) 12835–12842, https://doi.org/10.1039/C7NR03276E.
[49] C.N. Shyam Kumar, C. Possel, S. Dehm, V.S.K. Chakravadhanula, D. Wang, W. Wenzel, R. Krupke, C. Kübel, Graphitizability of polymer thin films: an in situ TEM study of thickness effects on nanocrystalline graphene/glassy carbon formation, Macromol. Mater. Eng. (2023), https://doi.org/10.1002/mame.202300230.
[50] A. Riaz, F. Pyatkov, A. Alam, S. Dehm, A. Felten, V.S.K. Chakravadhanula, B. S. Flavel, C. Kübel, U. Lemmer, R. Krupke, Light emission, light detection and strain sensing with nanocrystalline graphene, Nanotechnology 26 (2015) 325202, https://doi.org/10.1088/0957-4484/26/32/325202.
[51] D. Alvira, D. Antorán, J.J. Manyà, Plant-derived hard carbon as anode for sodium-ion batteries: a comprehensive review to guide interdisciplinary research, Chem. Eng. J. 447 (2022), https://doi.org/10.1016/j.cej.2022.137468.
[52] C. Kumar Shyam, Neelakandhan, In Situ TEM Studies on the Graphitization and Growth of Nanocrystalline Graphene from Polymers, 2019, p. 147.
[53] J.G. Simmons, Generalized formula for the electric tunnel effect between similar electrodes separated by a thin insulating film, J. Appl. Phys. 34 (1963) 1793–1803, https://doi.org/10.1063/1.1702682.
[54] X.W. Zhang, Y. Pan, Q. Zheng, X.S. Yi, Time dependence of piezoresistance for the conductor-filled polymer composites, J. Polym. Sci. B Polym. Phys. 38 (2000) 2739–2749, https://doi.org/10.1002/1099-0488(20001101)38:21<2739::AID-POLB40>3.0.CO;2-O.
[55] J. Zhao, C. He, R. Yang, Z. Shi, M. Cheng, W. Yang, G. Xie, D. Wang, D. Shi, G. Zhang, Ultra-sensitive strain sensors based on piezoresistive nanographene films, Appl. Phys. Lett. 101 (2012), https://doi.org/10.1063/1.4742331.